Check for updates

BIOELECTRICITY
Volume 00, Number 00, 2026
Mary Ann Liebert, A Part of Sage
© The Author(s)
DOI: 10.1177/25763113261426295

Microdosimetric Calibration of Microsecond Pulsed Electric Field Stimulation Across Electrodes Technologies for the RISEUP Project

Sara Fontana, PhD,[1,*] Noemi Dolciotti, PhD,[1,*] Amir Ghassabi, MSc,[1] Laura Caramazza, PhD,[1] Irene Cuenca-Ortolá, MSc,[2] Manuel Monleon-Pradas, PhD,[2] Fernando Gisbert Roca, PhD,[2] Micol Colella, PhD,[1] Alessandra Paffi, PhD,[1] Franck M. André, PhD,[3] Claudia Consales, PhD,[4] Francesca Apollonio, PhD,[1] and Micaela Liberti, PhD[1]

Abstract

RISEUP, short for *Regeneration of Injured Spinal Cord by Electro Pulsed Bio-Hybrid Implant*, is a European project aimed at offering a real possibility of recovery after spinal cord injury. This approach leverages highly intense microsecond pulsed electric fields (μsPEFs) to transiently permeabilize cellular membranes, thereby guiding stem cells proliferation and differentiation pathways. *In vitro* experiments are underway to develop an optimized stimulation protocol. An initial experimental phase employed faced electrodes (FE), while a second phase uses cylindrical electrodes (CE), corresponding to electro pulsed bio-hybrid (EPB) device - *Prototype 0*. Since the two configurations generate different electric (E-) field distributions, a numerical calibration of the voltage applied to the CE system was required. The objective of this calibration is to ensure that the E-field intensities generated between the CE electrodes match those previously shown to induce electroporation responses in stem cells with the FE setup. Numerical models of both FE and CE were implemented in COMSOL Multiphysics, and a calibration procedure was fine-tuned to ensure that the CE setup produced an average electric field comparable to the 30 kV/m value achieved by the FE system. The calibration process adjusted the applied voltage in the CE system from the nominal 15 V to 35.4 V to achieve a median electric field of 30 kV/m within the extracellular matrix volume that will host the stem cells. Following this, a microdosimetric study using advanced 3D virtual stem cells, including intracellular compartments, was performed to validate the calibration. The study confirmed that the two systems produced comparable electroporation effects, as evidenced by similar transmembrane potentials and pore densities on both plasma and intracellular membranes. The developed calibration methodology effectively harmonizes the stimulation conditions between different electrodes technologies employed in the RISEUP project, providing crucial support for optimizing *in vitro* protocols during experimental phases.

Keywords: electrodes calibration, pulsed electric field stimulation, microdosimetry, stem cells, spinal cord injury regeneration

Introduction

The spinal cord (SC) is an afferent structure of the central nervous system (CNS) that serves as a messenger between the brain and the rest of the body.[1] Traumas or degenerative pathologies may lead to spinal cord injury (SCI),[2] leading to an irreversible degradation of bodily movements, sensory perception, and the autonomous regulation of vital functions.[3,4]

Among the innovative treatments under development, the most promising research fields focus on the electroceuticals approach,[5] as well as on stem cells-based applications to stimulate regenerative processes on the damaged tissue.[6] For what concerns the electroceuticals, significant interest has

[1]Department of Information Engineering, Electronics and Telecommunications (DIET), Sapienza University of Rome, Rome, Italy.
[2]Center for Biomaterials and Tissue Engineering, Universitat Politècnica de València, Valencia, Spain.
[3]UMR 9018 METSY, CNRS, Université Paris-Saclay, Gustave Roussy, Villejuif, France.
[4]Division of Health Protection Technologies, ENEA-Italian National Agency for New Technologies, Energy and Sustainable Economic Development, Rome, Italy.
*Author Sara Fontana and Noemi Dolciotti contributed equally to this work.

been directed toward developing techniques that employ various forms of electrical stimulation, to leverage the residual supraspinal connections below the injury site.[7] Epidural electrical stimulation shows promise in restoring movement and autonomic functions after SCI.[7,8] Alternatives like transcutaneous epidural stimulation,[9,10] peripheral nerve stimulation[11,12] offer noninvasive therapeutic options, whereas functional electrical stimulation,[13,14] and cortical stimulation[15] are exploited in the rehabilitation stage.

Another alternative patch is represented by stem cells-based therapies, that offer a promising approach to promote neurogenesis following SCI. This approach harnesses the capabilities of various types of undifferentiated stem cells to reduce inflammation, support neuronal survival, and release neurotrophic factors.[4,6,16–19]

Many research groups are putting in a huge effort to find resolutive solutions for SCI treatment. Among them, the European Project *Regeneration of Injured Spinal Cord by Electro Pulsed Bio-Hybrid Implant* (RISEUP) aims at the regeneration of the injured SC through the development of a biocompatible and implantable electro pulsed bio-hybrid (EPB) device that supports and guides the differentiation of human induced neural stem cells (iNSCs) combined with mesenchymal stem cells (MSCs). The final goal is to effectively create a bio-hybrid cell bridge over the damaged area, fostering axonal regeneration, a key factor in functional recovery. Given the complex mechanisms involved in RISEUP, the EPB has been engineered to meet two key requirements: providing a nurturing and guiding environment to support stem cells growth, differentiation, and migration, and delivering effective electrical stimulation to influence stem cells fate. The EPB integrates an array of gold planar and interdigitated electrodes on a polylactic acid (PLA) substrate, overlaid with a biocompatible PLA microfibrils' scaffold. iNSCs and MSCs will be seeded on the scaffold within an extracellular medium (ECM) and exposed to microsecond duration pulsed electric field (μsPEF) to promote their proliferation and differentiation in neuronal lineage, via electroporation-mediated modulation of calcium ions fluxes across the plasma and endoplasmic reticulum (ER) membranes.[20–24]

The EPB development has progressed through several stages of design optimization and refinement (as described in Fontana et al.,[25]). While the EPB was still under development, it was necessary to start *in vitro* experiments early in the project to preliminary investigate the effects of μsPEF stimulation on stem cells and to establish a robust stimulation protocol for future *in vivo* experiments. In a preliminary phase of *in vitro* experiments, a technology of titanium planar and parallel electrodes (Faced Electrodes, FE) was used, since it was a well-known and readily available system for preliminary experiments on stem cells cultures.[24] Subsequently, *in vitro* experiments moved to the use of gold cylindrical electrodes (CE), which represent the EPB - *Prototype 0*, an early version of the EPB device comprising pairs of cylindrical alternating active and ground electrodes, overlaid with a PLA microfibrils lane. However, the two electrodes configurations generate markedly different electric (E-) field distributions: the FE setup produces a homogeneous E-field, different from the one induced in the EPB as shown in Fontana et al.,[25] whereas the CE configuration results in a heterogeneous E-field, also due to the microfibrils' presence. Consequently, calibration of the CE was required to ensure that, under *in vitro* conditions, the delivered stimulation elicited biological effects on stem cells consistent with those observed in the earlier FE-based *in vitro* experiments.

The aim of this work is to develop a calibration method that accounts for the heterogeneous E-field in the CE, by numerically estimating in COMSOL Multiphysics the E-field distributions in both FE and CE. The calibration procedure aims to establish the CE stimulation to deliver an average E-field of 30 kV/m within the ECM volume where the stem cells will be exposed, by applying a bipolar pulse with 25 μs + 25 μs duration, accordingly with the *in vitro* experiments reported in Vallet et al.[26] Subsequently, the calibration methodology will be validated using a mixture of 10 advanced 3D virtual stem cells to ensure comparable stimulation results between FE and CE.

Methods and Procedures

Faced electrodes and cylindrical electrodes numerical models

The FE system consists of a pair of parallel titanium electrodes, each 20 mm high and spaced 10 mm apart, as shown in Figure 1, Panel A.[24] In contrast, the CE system comprises three pairs of alternating active and ground electrodes made of gold, each with a diameter of 50 μm, a length of 4 mm, and an interelectrode distance of 500 μm (Fig. 1, Panel B). A microfibril lane, composed of fibers with a diameter of 10 μm,[25] is positioned above the electrodes at a height of approximately 112 μm, determined by the thickness of the supporting structure.

Both electrode configurations were modeled in COMSOL Multiphysics (v. 6.1). For the FE simulation, to reduce computational complexity while avoiding spurious capacitive effects, the electrode spacing was reduced from 10 mm to 2000 μm (data not shown). A representative subdomain was modeled using periodic boundary conditions (PBCs) on the *zy* external faces, allowing the reduced domain (Fig. 1, Panel C) to emulate the behavior of the full-size setup shown in Figure 1, Panel A. The ECM region, where cells are to be embedded, was included in the simulation. For the CE system, the simulation domain shown in Figure 1, Panel D represents a single pair of active (red) and ground (green) electrodes embedded in a PLA substrate. The overlying microfibril monolayer, modeled according to Fontana et al.,[25] is also included. To reproduce the effects of the complete electrode array, PBCs were applied to the *zx* and *zy* faces, enabling the single-pair model to capture the full CE configuration's field distribution. All the materials properties are reported in Table 1. It is important to highlight that the same ECM is used in both FE and CE configurations to host a mixed population of MSCs and iNSCs.

Rationale of the E-field numerical calibration

To define the stimulation parameters, ensuring consistent biological effects across different electrode systems, a numerical calibration of the E-field was performed.

In the FE system, a homogeneous E-field of 30 kV/m was established by applying a bipolar pulse (25 μs + 25 μs, with rise/fall time of 2.5 μs), as previously tested *in vitro*.[26] Figure 2, Panel A (top), shows the corresponding E-field distribution. The field vectors indicate direction and magnitude

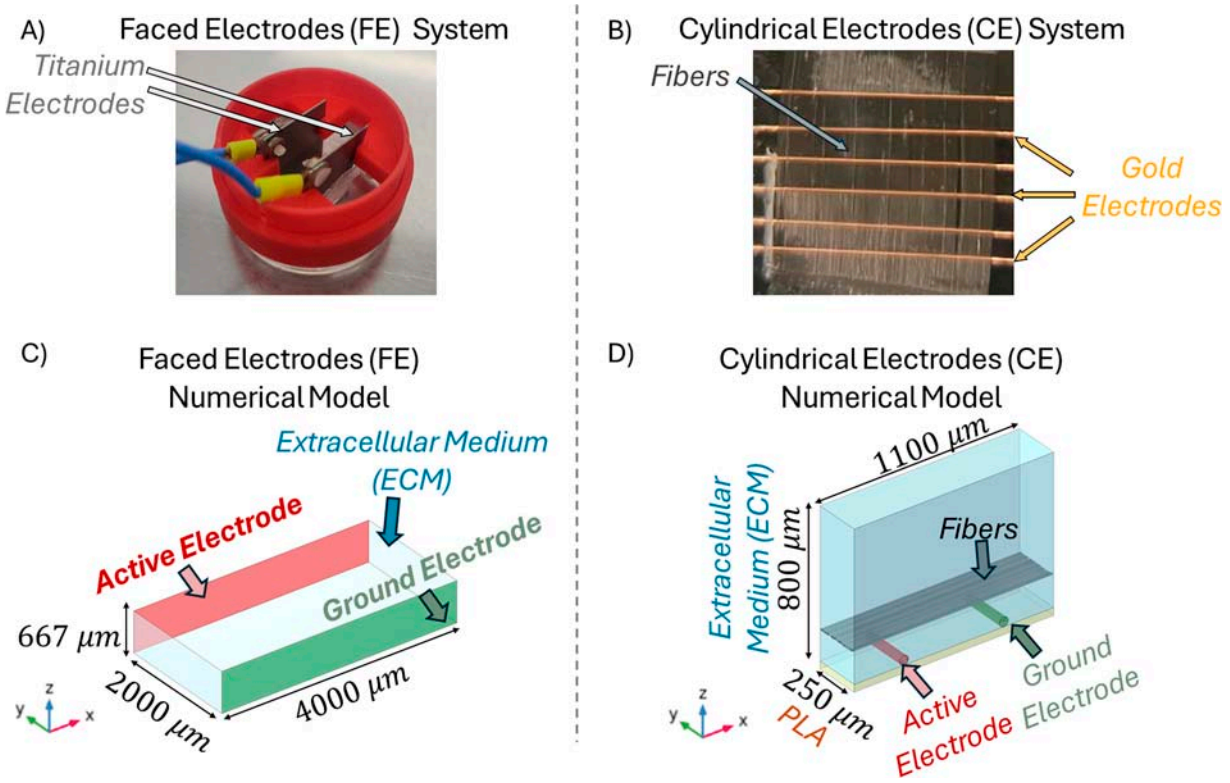

FIG. 1. *In vitro* exposure systems within RISEUP: Faced Electrodes **(A)**, Cylindrical Electrodes **(B)** and the relative numerical models in Comsol Multiphysics **(C)** and **(D)**, respectively.

(length), and their uniformity, highlighted by the consistent length and parallel orientation, confirms the homogeneity of the field within the ECM hosting the cells.

In contrast, the CE system, when driven with the same pulse shape and a nominal voltage of 15 V applied across the electrodes spaced 500 μm apart, produces a non-uniform E-field, as illustrated in Figure 2, Panel A (bottom). The field originates from the active electrodes and radiates toward the ground electrodes, decreasing in intensity with distance. The presence of PLA microfibrils causes slight field attenuation due to their insulating nature, yet a bridging effect across the interfibrillar spaces still allows field propagation, as discussed in Fontana et al.[25]

For both configurations, the calibration focused on the ECM volume designated to place the virtual stem cells mixture, highlighted by the white rectangles in Figure 2, Panel A, at the base of the FE system and above the fibril layer in the CE system. Notably, this ECM volume is dimensioned to fit the virtual mixture (that will be introduced in the next section) and is identical for both CE and FE systems.

E-field values were extracted from the ECM volume hosting the stem cells and analyzed statistically using boxplots (Fig. 2, Panel B). For the CE system, the initial nominal 15 V input yielded a median E-field of 12.7 kV/m, insufficient to match the FE reference. Based on this, the applied voltage was adjusted to 35.4 V, achieving a median E-field of 30 kV/m within the same target volume, given the voltage-to-field linear relationship.

Figure 2, Panel C, presents cross-sectional E-field maps on multiple *xy* planes within the ECM of the calibrated CE model. These maps visualize the E-field gradients and validate the spatial exposure conditions that stem cells will experience *in vitro*. The calibration thus ensures a comparable stimulation environment between FE and CE systems, critical for consistent electroporation outcomes across experiments.

Table 1. Dielectric Properties of Materials Used in FE, CE and Virtual Stem Cells Models

Component	σ *[S/m]*	ε_r
Extracellular Matrix (ECM)	1.61	242
PLA	$4.25 \cdot 10^{-11}$	$6.75 + j \cdot 0.038$
Titanium	$7.407 \cdot 10^{5}$	1
Gold	$45.6 \cdot 10^{6}$	1
Plasms	0.3	67
Plasma, ER and mito membranes	$1.1 \cdot 10^{-7}$	11.7
Nucleus Membrane	$8.3 \cdot 10^{-5}$	11.7

Fine-tuning of the microdosimetric study to validate the E-field calibration

Once the E-field has been calibrated, it is necessary to prove that the calibration performed can guarantee stimulation results on stem cells that are in line with those obtained with the FE. A microdosimetric study, coupled with the electroporation model, was carried out through advanced 3D virtual MSCs and iNSCs, including also intracellular structures, reconstructed from real confocal microscopy images. MSCs models were previously developed in De Angelis et al.,[27] with a MATLAB custom-made procedure, including cytoplasm,

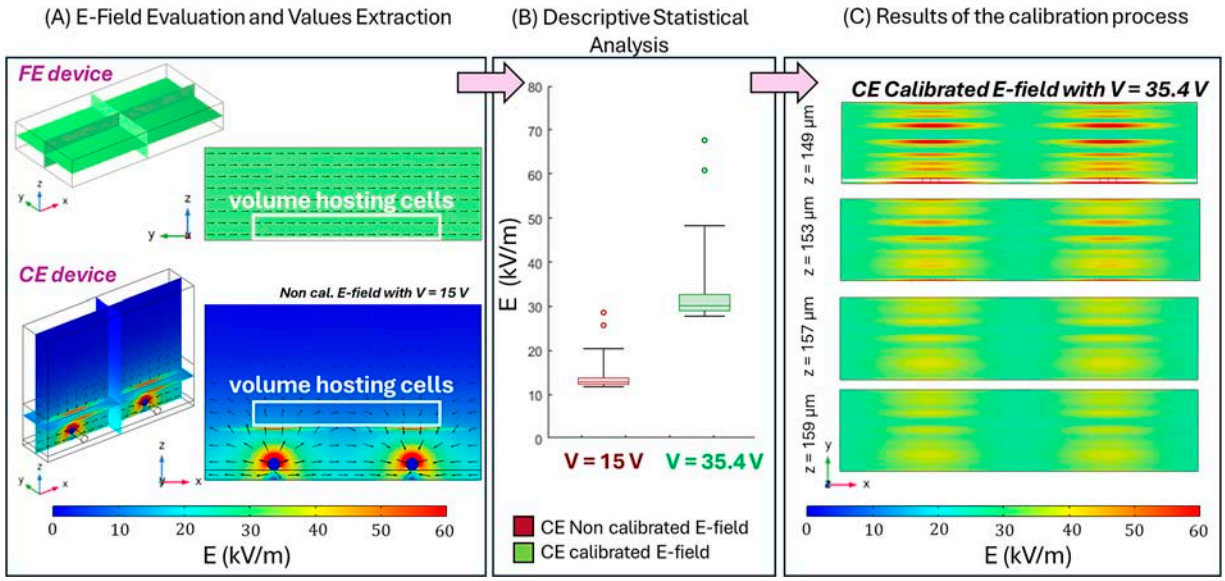

FIG. 2. Rationale of the E-field numerical calibration without cell. **(A)** Non calibrated E-field evaluation FE (upper row) and CE (bottom row) induced by a 25 µs-bipolar pulse. The ECM volume hosting stem cells, taken as a reference to start the calibration process, has been highlighted with the white box. **(B)** Descriptive statistical analysis to define the stimulation intensity: boxplot of E-field in the whole volume hosting cells of CE device, showing the lower and upper whiskers corresponding to the 1st and 99th percentiles, the interquartile range (25th–75th percentiles), and the 99.9th and 99.99th percentiles displayed as outliers. **(C)** Results of the calibration process: E-field distribution of different axial planes in the CE device volume where the cells will be hosted.

nucleus, and ER compartments. Virtual iNSCs were instead generated from high resolution confocal microscopy images using a dedicated semi-automatic reconstruction procedure.[28,29] The models include cytoplasm, nucleus, ER, and mitochondria. The cells are imported in COMSOL Multiphysics, duplicated, and placed close to each other to represent a mixture composed of 6 iNSCs and 4 MSCs (Fig. 3, Panel C), for a total of 10 virtual stem cells. Cell density and spatial arrangement were selected to represent the packed mixture under *in vitro* conditions. The same mixture composition, density, and relative positioning were intentionally adopted in both FE and CE configurations in order to isolate the effect of electrode geometry and E-field calibration. The mixture is then placed adherent to the FE basis (Fig. 3, Panel A) and over the microfibrils in the CE (Fig. 3, Panel B), to well represent the experimental exposure conditions. Due to the complexity and the realism of both models, the geometries have been further reduced. Specifically, in addition to PBCs, symmetry planes (SPs) were applied on the *yz* faces created by cutting through the center of the CE electrodes, to represent the

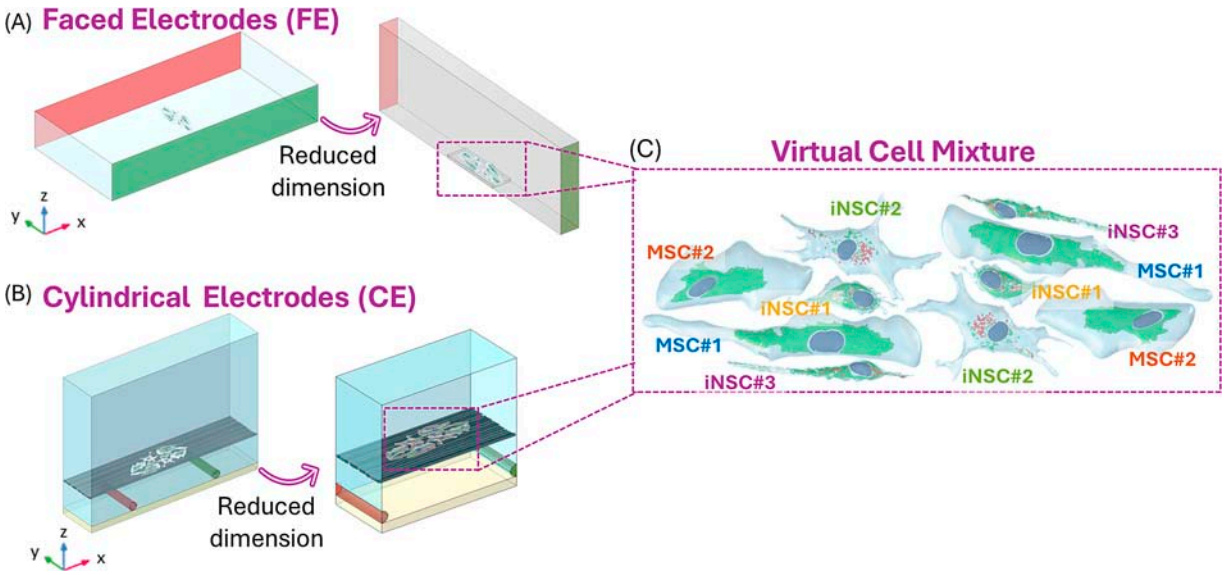

FIG. 3. Advanced numerical models for electrodes' calibration: mixture of 10 cells inside the FE **(A)**, adherent to the basis of the device, and inside the CE **(B)**, supported by the microfibrils, with a focus on the cells used to recreate the mixture **(C)**.

larger experimental domain while keeping computational cost manageable, with the solution on one side mirrored to the opposite side.[28] This allows the small simulated unit to effectively replicate the cell mixture in the full FE and CE systems. All the dielectric properties assigned are reported in (Table 1) and are consistent with.[28–30]

The multiphysics problem is implemented by solving the electric problem, related to the bipolar μsPEF application, using the AC/DC electric current (ec) module. The μsPEF stimulus induces the formation of hydrophilic pores in the cell membranes, leading to an increase in membrane conductivity, as described in literature by the Smoluchowski equation:[31]

$$\frac{dN}{dt} = \alpha e^{\left(\frac{TMP}{Vep}\right)^2} \cdot \left(1 - \frac{N}{N_0} e^{-q\left(\frac{TMP}{Vep}\right)^2}\right) \quad (1)$$

where N represents the pore density per mm^2, with the transmembrane potential (TMP) computed by the ec module serving as the input variable. An additional term accounting for the increase in membrane conductivity σ_{ep} is added to the conductivity of the unporated membrane, as follows:

$$\sigma_m = \sigma_{m0} + N \cdot \frac{2\pi r_p^2 \sigma_p h}{\pi r_p + 2h} \quad (2)$$

In the equation (2), r_p is the pore radius, h is the membrane thickness of 5 nm and σ_p is the pore conductivity,[32] expresses as:

$$\sigma_p = \frac{\sigma_e - \sigma_i}{\ln\left(\frac{\sigma_e}{\sigma_i}\right)} \quad (3)$$

where σ_e is the ECM conductivity and σ_i is the cytoplasm conductivity (Table 1). All the parameters used in equations (1), (2) and (3) are reported in Table 2.[28,29]

TABLE 2. PARAMETERS USED TO IMPLEMENT THE PORE FORMATION DYNAMICS

Name	*Symbol*	*Value*
Equilibrium Pore Density	N_0	$1.5{\cdot}10^9\ m^{-2}$
Electroporation Parameter	α	$5{\cdot}10^{11}$
Characteristic Electroporation Voltage	V_{ep}	258 mV
Electroporation Constant	q	2.46
Pore Radius	r_p	0.76 nm

Results

To demonstrate the effectiveness of the applied calibration methodology, this section presents the results in terms of electrical quantities, such as the induced E-field and TMP, as well as the resulting N after μsPEF stimulation, for both FE and CE. Figure 4 shows the calibrated E-field distribution for an applied field of 30 kV/m on a selected *xy* plane intersecting the cell mixture and across the cytoplasm volume, in FE (Panels A and C) and CE (Panels B and D), at the beginning of the pulse (t = 9 μs). In the absence of cells, the FE configuration exhibits a highly uniform E-field distribution (Panel A), both in intensity and direction, as expected for parallel electrodes. In contrast, the CE configuration shows a spatially varying E-field intensity (Panel B) also due to the microfibrils presence, while preserving a well-defined and predominantly uniform field direction, as highlighted by the arrow plots. In the FE configuration, the introduction of the cell mixture (Panel C) locally perturbs the otherwise homogeneous field, resulting in a pronounced shielding effect within the cluster. However, the E-field direction remains largely aligned with the applied field, indicating that the perturbation primarily affects the field intensity rather than its orientation. Comparable behavior is observed in the CE configuration (Panel D), where the proximity and spatial

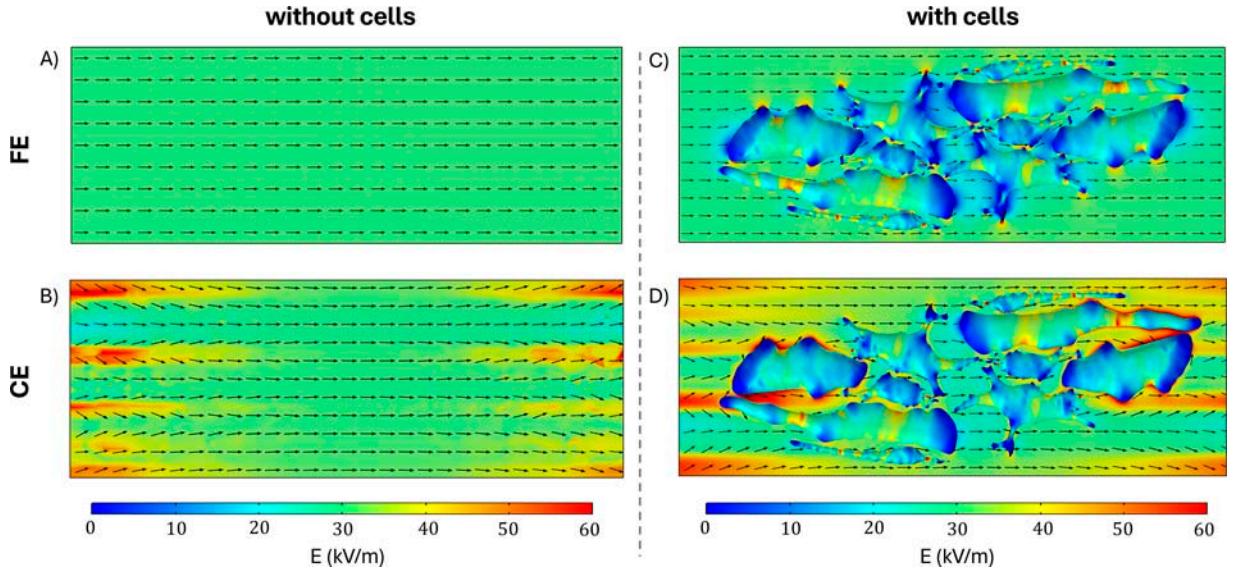

FIG. 4. E-field distribution and vector field representation without and with cells. Maps report E-field on a *xy* plane in FE **(A, C)** and CE **(B, D)**. In the presence of cells, the E-field distribution is also reported within the cytoplasm volume (FE: C; CE: D). Arrows indicate the local E-field direction. The E-field distribution is shown at the onset of the positive pulse (t = 9 μs).

arrangement of the cells lead to local E-field distortions. Despite the presence of microfibrils and geometric confinement, the arrows indicate that the E-field direction remains consistent and it is able to effectively penetrate the cell cluster. When properly calibrated, the CE configuration induces intracellular E-field levels comparable to those observed in the FE system. Overall, despite the different electrodes geometries and spatial field distributions, the E-field experienced by the cells within the mixture is comparable between FE and CE configurations. These results are further confirmed by the temporal evolution of the averaged E-field (Fig. 5), computed over the cytoplasm volume of each pair of the same cells type (for instance, averaged over the two MSC#1 cytoplasm). Overall, the E-field temporal profiles are consistent between the FE (on the left column) and CE (on the right column), confirming that the calibration methodology ensures a comparable exposure of each cell type to the applied field, despite the structural differences between the two environments. For instance, in the MSC#1 cytoplasm (blue curve), the peak E-field reaches values around 40 kV/m, with similar temporal decay in both FE and CE cases. In the internal compartments, the induced E-field values are lower due to the internal cellular shielding, yet the trends remain in agreement between FE and CE, reinforcing the robustness of the calibration.

Building on these observations, TMP maps on the plasma membrane surfaces are presented in Figure 6, where the active electrode is shown in red and the ground electrode in green. The TMP distribution shows good agreement between the FE (Panel A) and CE (Panel B) configurations, particularly in regions where TMP reaches values up to 1 V. In addition, the average TMP calculated on the plasma, ER, and mitochondrial membranes for each cell type pair is reported in Supplementary Fig. S1. As expected, the pore density closely follows the TMP distribution and shows a comparable pattern between FE (Panel C) and CE (Panel D). It is worth noting that the pore density reaches adequate levels up to 10^{14} m^{-2} on the plasma membranes, while the pore formation in the membranes of the inner compartments remains negligible (data not shown).

For this reason, the E-field intensity was increased to 100 kV/m. This enabled both verification of whether the calibration remained effective at higher field strengths and the assessment of whether the induced TMP and pore density on inner membranes would still exhibit consistent patterns between FE and CE. Supplementary Fig. S2 shows E-field for FE (Panel A) and CE (Panel B) on *xy* maps crossing the cells and on cells' volumes. The distributions are still in line between the two configurations, as confirmed by the averaged E-field in time in Supplementary Fig. S3. Figure 7 shows the TMP distribution in FE (Panel A) and CE (Panel B) at 100 kV/m, and, notably, the TMP reaches 1 V in the ER of MSC#1 and MSC#2 and in smaller areas of iNSC#1 and iNSC#3 (averaged TMP in time in Supplementary Fig. S4). The N in FE (Panel C) and CE (Panel D) results in similarly localized regions with pore densities up to 10^{14} m^{-2}, consistent between the two exposure conditions.

Discussion

This work presents the development and verification of a numerical calibration methodology aimed at harmonizing

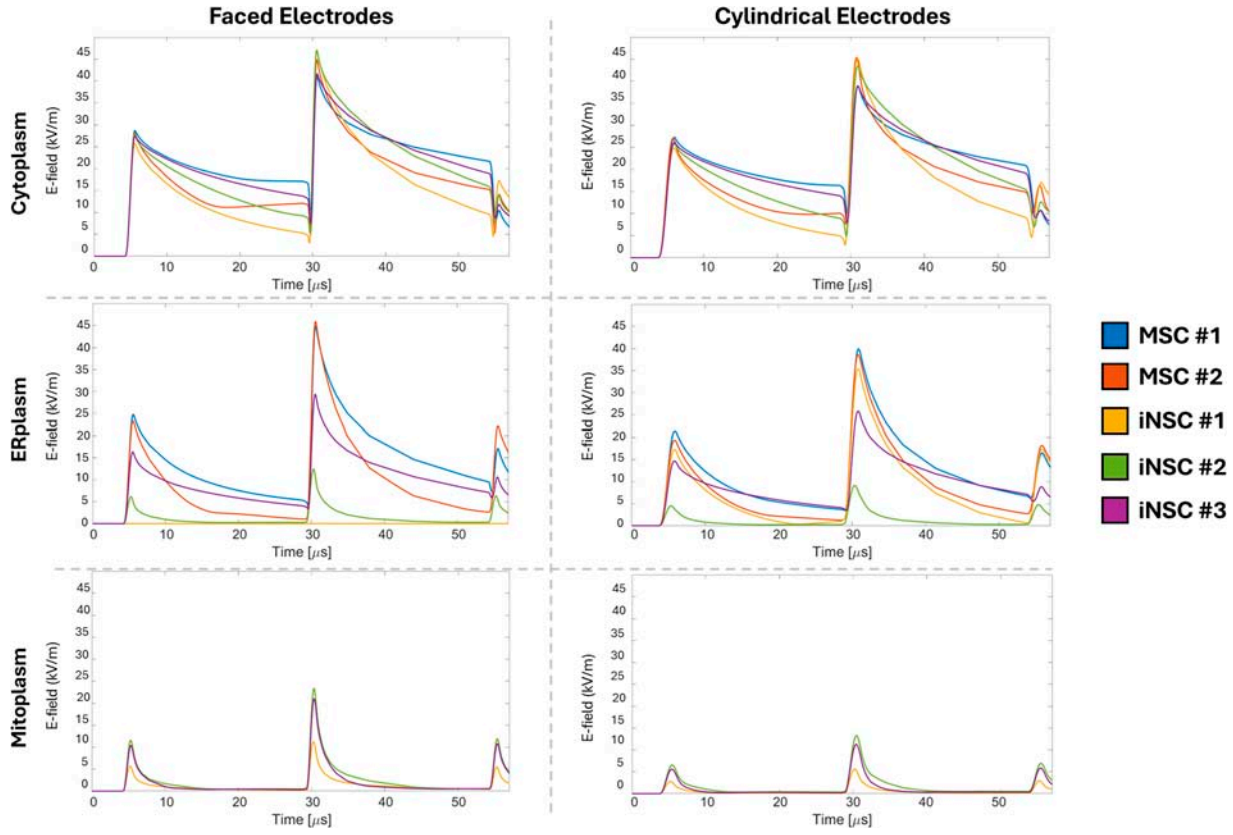

FIG. 5. E-field distribution in the cellular compartments in time in both systems at 30 kV/m. Each curve represents the average E-field for a specific cell type.

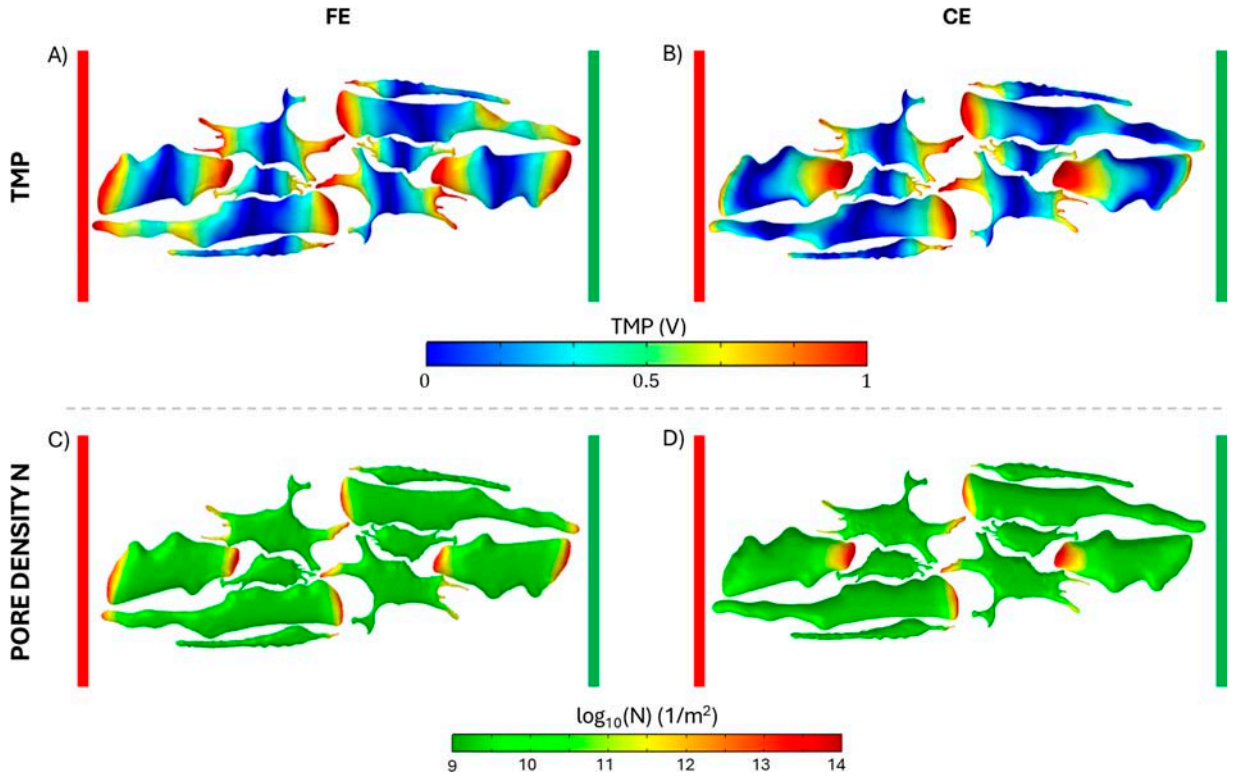

FIG. 6. TMP distribution at the beginning of the pulse on plasma membranes at 30 kV/m for FE **(A)** and CE **(B)**. Pore density at the end of the pulse for FE **(C)** and CE **(D)**. (Figures not in scale).

the E-field exposure between two electrode configurations, FE and CE, to ensure consistent biological effects of μsPEF stimulation on stem cells, thereby enabling the transition from early *in vitro* experiments to the advanced EPB prototype. The obtained results demonstrate that the developed calibration methodology ensures consistent electrical exposure

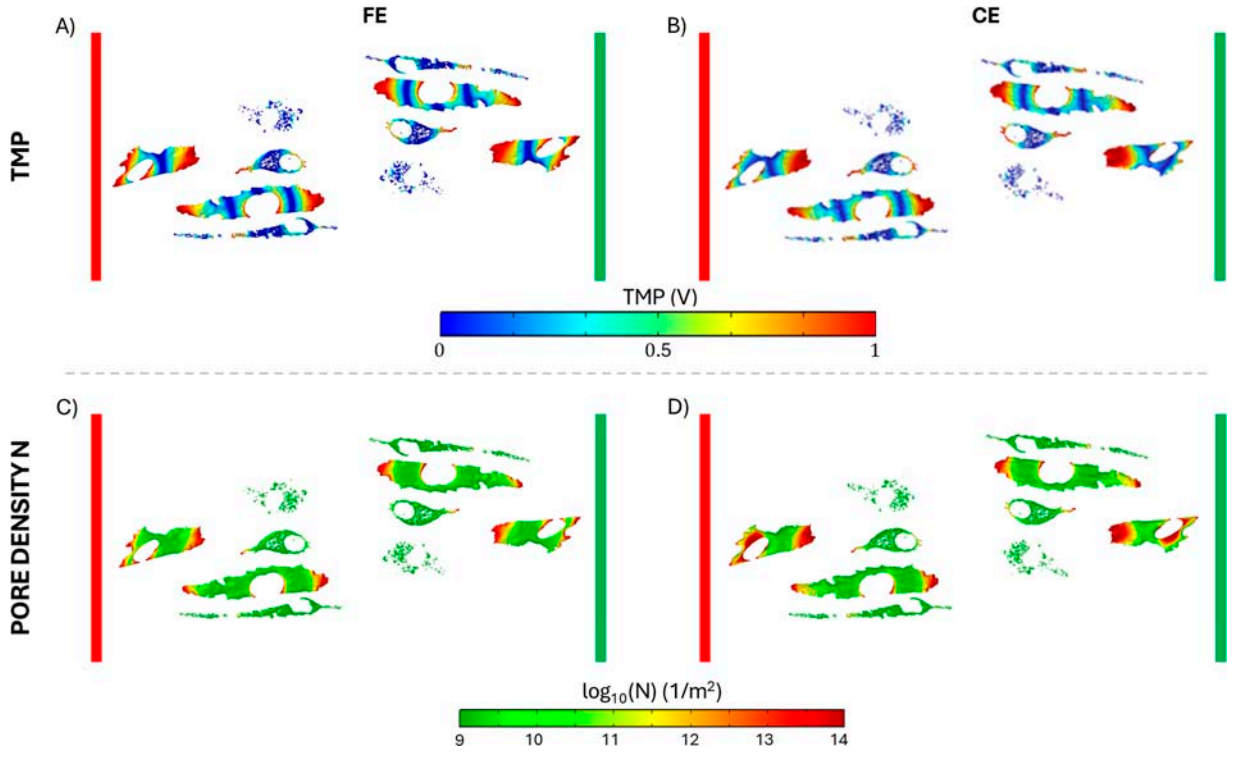

FIG. 7. TMP at the beginning of the pulse on inner membranes at 100 kV/m for FE **(A)** and CE **(B)**. Pore density at the end of the pulse for FE **(C)** and CE **(D)**. (Figures not in scale).

between the two electrodes systems, despite substantial differences in structure and E-field distribution. Numerical calibration allowed to identify an applied voltage value in the CE system, i.e., 35.4 V, capable of generating a median E-field of 30 kV/m within the ECM volume hosting stem cell mixture, comparable to the homogeneous field produced by the FE system. Verification using advanced microdosimetric models confirmed the validity of this approach: E-field, TMP and N on the plasma and intracellular compartments show similar behavior between the two configurations. In particular, the effectiveness of the proposed calibration methodology ultimately emerges from the quantitative comparison of electroporation outcomes across electrode configurations, summarized in Figure 8.

The E-field bridging effect observed in the CE system is an interesting aspect, as it could promote locally more intense exposure and therefore potentially more effective stimulation of desired biological processes.[25] Furthermore, the results obtained at higher fields (100 kV/m) show that the consistency between FE and CE is maintained even under more intense stimulation conditions, with TMP and N consistent in intracellular compartments.

A quantitative synthesis of the calibration outcome is provided by the boxplots reported in Figure 8. By directly comparing pore density distributions across cell types and electrodes configurations, Figure 8 captures the effective intracellular outcome of the stimulation, reducing the influence of local field inhomogeneities. At 30 kV/m, the distributions of N on the plasma membranes (Panel A) demonstrate strong agreement across the two configurations, confirming the efficacy of the calibration at standard exposure levels. At 100 kV/m, the ER membrane pore densities (Panel B) become appreciable, especially in MSCs, indicating deeper intracellular engagement while still maintaining close agreement between the FE and CE systems.

In this study, a single configuration of the cell mixture was considered, with fixed orientation, density, and relative positioning. This choice is consistent with the primary objective of the work, which is the development and validation of a numerical calibration methodology between different electrode configurations. The potential influence of alternative cell arrangements or spacing on intracellular exposure patterns may be investigated in future studies. These quantitative comparisons support the robustness of the calibration approach across varying stimulation intensities and cell compartments, underscoring the reliability of the CE configuration as a valid and scalable solution for future *in vitro* and translational applications within the RISEUP project.

Conclusion

The observed alignment of the stimulation results supports the conclusion that the E-field is well calibrated across both configurations. This ensures a reproducible, controlled, and biologically meaningful exposure of the stem cell mixture, validating the reliability of the calibration approach. Such harmonization of stimulation conditions is critical for the progression of the RISEUP project, guaranteeing continuity and comparability between the two *in vitro* experiments conducted with FE and the CE device, that is, EPB - *prototype 0*.

Moreover, the integration of advanced 3D virtual stem cells has proven instrumental in the calibration process, offering detailed insights into intracellular electroporation dynamics and enabling rigorous, microdosimetry-based

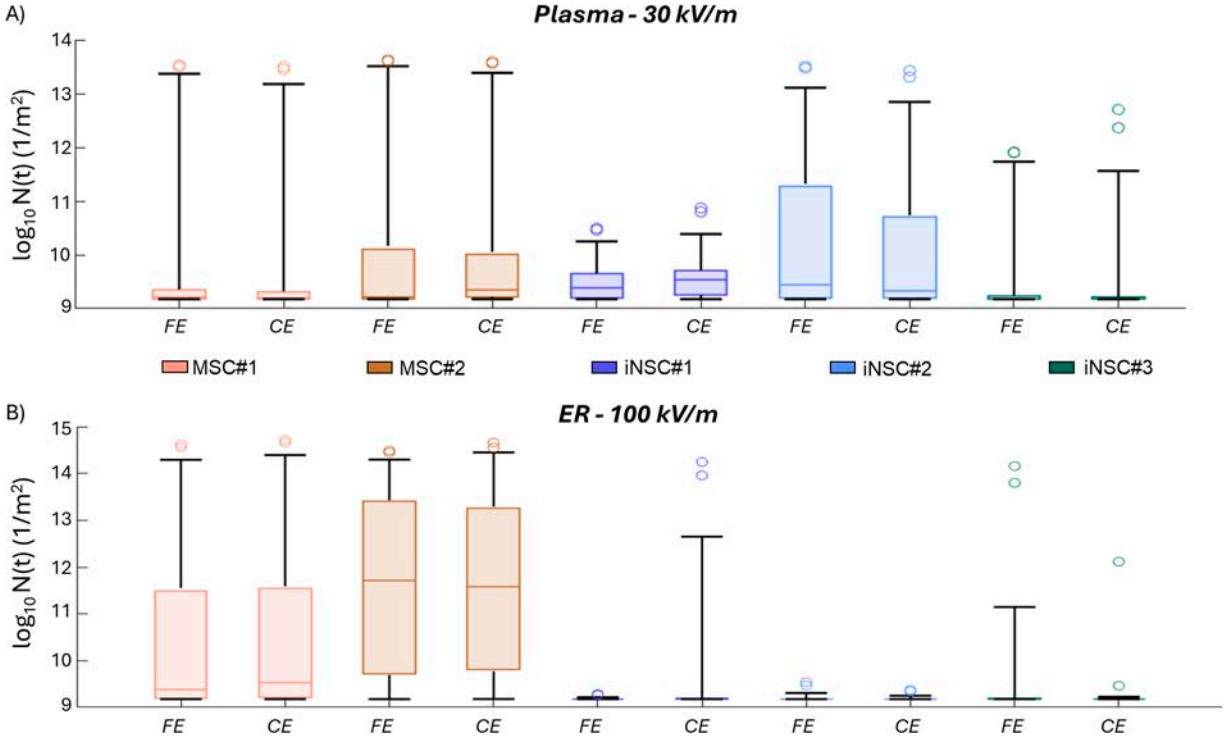

FIG. 8. Pore density boxplot at the end of the pulse on plasma membranes for 30 kV/m **(A)**, and on inner membranes for 100 kV/m **(B)**. The bloxplot show the lower and upper whiskers corresponding to the 1st and 99th percentiles, the interquartile range (25th–75th percentiles), and the 99.9th and 99.99th percentiles displayed as outliers.

validation of the exposure conditions. This digital twin-based approach not only strengthens confidence in the calibration results, but also opens the way for predictive and personalized refinements of stimulation protocols. The quantitative agreement observed in the pore density distributions across electrode configurations, as summarized in Figure 8, confirms the robustness of the proposed calibration strategy at the intracellular level.

Overall, the proposed methodology constitutes a robust and transferable framework for numerical calibration and exposure standardization, applicable to a wide range of complex electrode-based systems. By ensuring consistent and quantifiable biological effects across differing technological platforms, it provides a foundational tool to support reproducibility, comparability, and translational relevance in bioelectrical stimulation broader field.

Authors' Contributions

S.F. and N.D.: Writing—original draft, data curation and visualization. S.F., N.D., L.C., F.A., and M.L.: Methodology and software. S.F., N.D., A.G., L.C., I.C.O., M.C., and A.P.: Formal analysis. S.F., N.D., F.A., and M.L.: Conceptualization. S.F., N.D., L.C., M.M.P., F.G.R., F.M.A., C.C., F.A., and M.L.: Investigation. M.L. and F.A.: Supervision. C.C.: Project administration. All authors contributed writing—review and editing—the article and approved the submitted version.

Author Disclosure Statement

No competing financial interests exist.

Funding Information

This work has been developed in the framework of and supported by the FET-OPEN RISEUP project funded by the European Union's Horizon 2020 research and innovation program (grant agreement No. 964562).

Supplementary Material

Supplementary Figures

References

1. Tan S, Faull RLM, Curtis MA. The tracts, cytoarchitecture, and neurochemistry of the spinal cord. Anat Rec (Hoboken) 2023;306(4):777–819.
2. David G, Mohammadi S, Martin AR, et al. Traumatic and nontraumatic spinal cord injury: Pathological insights from neuroimaging. Nat Rev Neurol 2019;15(12):718–731.
3. Venkatesh K, Ghosh SK, Mullick M, et al. Spinal cord injury: Pathophysiology, treatment strategies, associated challenges, and future implications. Cell Tissue Res 2019; 377(2):125–151.
4. Rodríguez-Barrera R, Ibarra A, Rivas-González M, et al. Neurogenesis after spinal cord injury: State of the art. Cells 2021;10(6):1499.
5. Famm K, Litt B, Tracey KJ, et al. A jump-start for electroceuticals. Nature 2013;496(7444):159–161.
6. Damianakis EI, Benetos IS, Evangelopoulos DS, et al. Stem cell therapy for spinal cord injury: A review of recent clinical trials. Cureus 2022;14(4):e24575.
7. Dorrian RM, Berryman CF, Lauto A, et al. Electrical stimulation for the treatment of spinal cord injuries: A review of the cellular and molecular mechanisms that drive functional improvements. Front Cell Neurosci 2023;17:1095259.
8. Wagner FB, Mignardot J-B, Le Goff-Mignardot CG, et al. Targeted neurotechnology restores walking in humans with spinal cord injury. Nature 2018;563(7729):65–71.
9. Taylor C, McHugh C, Mockler D, et al. Transcutaneous spinal cord stimulation and motor responses in individuals with spinal cord injury: A methodological review. PLoS One 2021;16(11):e0260166.
10. Islam MA, Zaaya M, Comiskey E, et al. Modulation of soleus H-reflex excitability following cervical transspinal conditioning stimulation in humans. Neurosci Lett 2020;732: 135052.
11. Ong Sio LC, Hom B, Garg S, et al. Mechanism of action of peripheral nerve stimulation for chronic pain: A narrative review. Int J Mol Sci 2023;24(5):4540.
12. Kamboonlert K, Panyasriwanit S, Tantisiriwat N, et al. Effects of bilateral transcutaneous tibial nerve stimulation on neurogenic detrusor overactivity in spinal cord injury: A urodynamic study. Arch Phys Med Rehabil 2021;102(6):1165–1169.
13. Marquez-Chin C, Popovic MR. Functional electrical stimulation therapy for restoration of motor function after spinal cord injury and stroke: A review. BioMed Eng OnLine 2020;19(1):34; doi: 10.1186/s12938-020-00773-4
14. Karamian BA, Siegel N, Nourie B, et al. The role of electrical stimulation for rehabilitation and regeneration after spinal cord injury. J Orthop Traumatol 2022;23(1):2; doi: 10 .1186/s10195-021-00623-6
15. Choi EH, Gattas S, Brown NJ, et al. Epidural electrical stimulation for spinal cord injury. Neural Regen Res 2021; 16(12):2367–2375.
16. Kumamaru H, Lu P, Rosenzweig ES, et al. Regenerating corticospinal axons innervate phenotypically appropriate neurons within neural stem cell grafts. Cell Rep 2019;26(9): 2329–2339.e4.
17. Gazdic M, Volarevic V, Harrell CR, et al. Stem cells therapy for spinal cord injury. Int J Mol Sci 2018;19(4):1039.
18. Hussain G, Akram R, Anwar H, et al. Adult neurogenesis. Neural Regen Res 2024;19(1):6–15.
19. Ghosh HS. Adult neurogenesis and the promise of adult neural StemCells. J Exp Neurosci 2019;13.
20. Kawano S, Shoji S, Ichinose S, et al. Characterization of Ca2+ signaling pathways in human mesenchymal stem cells. Cell Calcium 2002;32(4):165–174.
21. Hanna H, Denzi A, Liberti M, et al. Electropermeabilization of inner and outer cell membranes with microsecond pulsed electric fields: Quantitative study with calcium ions. Sci Rep 2017;7(1):13079.
22. Vallet LA, André FM, Mir LM. Calcium oscillations in differentiating mesenchymal stem cells: Analysis and control using pulsed electric fields. In: 2021 XXXIVth General Assembly and Scientific Symposium of the International Union of Radio Science (URSI GASS), Rome, Italy. IEEE; 2021; pp. 1–4; doi: 10.23919/URSIGASS51995.2021.9560202
23. Innamorati G, Secchiaroli LC, Caramazza L, et al. Effects of the electromagnetic fields (EMFs) on cellular redox homeostasis. Free Radic Biol Med 2023;198:S8.
24. Innamorati G, Sanchez-Petidier M, Bergafora G, et al. Characterization of stem cells response to bipolar microsecond

pulses electric stimulation. Int J Mol Sci 2024;26(1):147; doi: 10.3390/ijms26010147
25. Fontana S, Caramazza L, Marracino P, et al. Electric field bridging-effect in electrified microfibrils' scaffolds. Front Bioeng Biotechnol 2023;11:1264406.
26. Vallet LA, Sánchez-Petidier M, Fernandes R, et al. Calcium oscillations in mesenchymal stem cells, a control on cell cycle progression to influence cell fate towards proliferation or differentiation? Stem Cell Res Ther 2025;16(1):446; doi: 10.1186/s13287-025-04454-8
27. De Angelis A, Denzi A, Merla C, et al. Confocal microscopy improves 3D microdosimetry applied to nanoporation experiments targeting endoplasmic reticulum. Front Bioeng Biotechnol 2020;8:552261; doi: 10.3389/fbioe.2020.552261
28. Dolciotti N, Fontana S, Caramazza L, et al. Microdosimetry - Driven optimization of μsPEF stimulation for stem cell neurogenesis in implantable bio - hybrid devices. Bioelectricity 2026; doi: 10.1177/25763113261428828
29. Fontana S, Dolciotti N, Moreno-Manzano V, et al. Microdosimetry of μsPEFs exposure on advanced stem cells 3D models in microfibrils' scaffolds. In: 2024 4th URSI Atlantic Radio Science Meeting (AT-RASC), Meloneras, Spain. IEEE; 2024; pp. 1–4.
30. Fontana S, Caramazza L, Colella M, et al. Advanced microdosimetric and neurofunctionalized multiphysics on stem cells models under microsecond pulse stimulation. IEEE J Electromagn RF Microwaves Med Biol 2024:1–10.
31. DeBruin KA, Krassowska W. Modeling electroporation in a single cell. I. Effects of field strength and rest potential. Biophys J 1999;77(3):1213–1224. Available from: https://www.cell.com/action/showFullText?pii=S0006349599769730
32. Mercadal B, Vernier PT, Ivorra A. Dependence of electroporation detection threshold on cell radius: An explanation to observations non compatible with schwan's equation model. J Membr Biol 2016;249(5):663–676.

Address correspondence to:
Micaela Liberti, PhD
Department of Information Engineering
Electronics and Telecommunications (DIET)
Sapienza University of Rome
Via Eudossiana 18
Rome
Lazio 00184
Italy

E-mail: micaela.liberti@uniroma1.it